J. Fluid Mech. (2003), *vol.* 481, *pp.* 385–411.
DOI: 10.1017/S0022112003003938 Printed in the United Kingdom

Direct numerical simulation of the sedimentation of solid particles with thermal convection

By HUI GAN[1], JIANZHONG CHANG[1], JAMES J. FENG[1] AND HOWARD H. HU[2]

[1]The Levich Institute for Physicochemical Hydrodynamics, City College of the City University of New York, New York, NY 10031, USA

[2]Department of Mechanical Engineering and Applied Mechanics, University of Pennsylvania, Philadelphia, PA 19104, USA

(Received 11 September 2002 and in revised form 6 December 2002)

Dispersed two-phase flows often involve interfacial activities such as chemical reaction and phase change, which couple the fluid dynamics with heat and mass transfer. As a step toward understanding such problems, we numerically simulate the sedimentation of solid bodies in a Newtonian fluid with convection heat transfer. The two-dimensional Navier–Stokes and energy equations are solved at moderate Reynolds numbers by a finite-element method, and the motion of solid particles is tracked using an arbitrary Lagrangian–Eulerian scheme. Results show that thermal convection may fundamentally change the way that particles move and interact. For a single particle settling in a channel, various Grashof-number regimes are identified, where the particle may settle straight down or migrate toward a wall or oscillate laterally. A pair of particles tend to separate if they are colder than the fluid and aggregate if they are hotter. These effects are analysed in terms of the competition between the thermal convection and the external flow relative to the particle. The mechanisms thus revealed have interesting implications for the formation of microstructures in interfacially active two-phase flows.

1. Introduction

Owing to their importance in innumerable industrial and natural processes, multiphase flows have been researched extensively. To some extent, however, the fact that multiphase flows are frequently accompanied by changes of phase or chemical reactions has been neglected. Obvious examples include boilers, combustors and slurry reactors. Currently, there is little theoretical understanding of multiphase flows undergoing phase change or reaction, and engineering design relies almost exclusively on empirical correlations (e.g. Smith, Stiegel & Ruether 1987). The difficulty of the problem stems from two mesoscopic features of such systems occurring on the length scale of individual particles or drops: (*a*) coupling between fluid flow and heat and mass transfer (HMT), the latter driven by interfacial activities; (*b*) the presence of moving and deforming interfaces and the interaction among neighbouring particles, drops or bubbles.

The earliest work on heat and mass transfer from individual particles assumed that the flow field is known and unaltered by the transport processes (Acrivos & Taylor 1962; see also Kovatcheva, Polyanin & Kurdjumov 1993). Research on coupling flow and HMT from a particle has largely been done in the context of drop combustion, where burning of vaporized fuel is coupled to the flow inside and

outside a translating drop (e.g. Ayyaswamy 1989; Sadhal, Ayyaswamy & Chung 1997). Thermal and compositional convection have been neglected in most of these studies, and the shape of the drop is assumed to remain spherical. The contributions cited above concern stationary single particles. Thus, the multiphase nature (*b*) is not taken into account. To our knowledge, HMT involving moving particles and/or deforming interfaces has been theoretically studied in only four papers. Huang & Ayyaswamy (1987) calculated the transient motion of a spherical droplet in a mixture of vapour and non-condensables while undergoing condensation. Juric & Tryggvason (1998) and Shin & Juric (2002) simulated film boiling on a heated plate. By tracking the position of the water–vapour interface, they were able to reproduce the detachment of vapour bubbles and the complex topological changes in the process. Hao & Prosperetti (2000) studied the motion of a vapour bubble in a non-uniform channel. The flow outside is taken to be a potential flow, and the pressure and the slip on the bubble's surface determine the condensation of the vapour.

Multi-particle systems with HMT have been theoretically studied only in the spray combustion literature; a comprehensive review may be found in Sirignano (1999). For regular arrays of a few droplets, numerical calculations have predicted the drag coefficient and Nusselt and Sherwood numbers, and the effect of droplet interaction has been examined (e.g. Chiang & Sirignano 1993). For sprays consisting of a large number of moving droplets, detailed information about the interface has to be sacrificed. Two types of models have been developed: the effective-continuum model and the trajectory model (Crowe 1991; Sirignano 1993). The former treats the droplets as an effective continuum and is in essence a generalized two-fluid model (Ishii 1975; Bennon & Incropera 1987). The latter recognizes the necessity of tracking discrete droplets, and achieves this by using correlations, say, for the drag and lift coefficients (Delnoij, Kuipers & van Swaaij 1997). In both models, the mass, momentum and heat transfer between the gas and the droplets must be provided as inputs; these may come from experimental data, phenomenological calculations using, say, the cell model (Bellan 1991), or accurate calculations for a single droplet (Sirignano 1999).

There are applications in which mesoscopic features are of little importance, and a continuum model suffices. This is the case, for instance, when the interfacial morphology is fixed or changes slowly as in heat exchangers with a melting front (Sasaguchi, Kusano & Viskanta 1997). Another example is a fluidized-bed reactor having millions of fine particles, where it is impractical and perhaps unnecessary to resolve the details on the particle length-scale (Dasgupta, Jackson & Sundaresan 1998). In general, however, heat and mass transfer and reaction rate are strong functions of the phase morphology, which, in turn, is dictated by the interaction among individual particles (Joseph 1996; Tirumkudulu, Tripathi & Acrivos 1999). Therefore, to achieve a fundamental understanding of interfacially active multiphase flows, we advocate a method of tracking individual particles via direct numerical simulations (DNS). By solving the momentum and energy equations with proper boundary conditions on phase boundaries, we compute the force, torque and heat flux on each particle and move them according to Newton's law of motion. Thus, we rationally account for the two mesoscopic features listed above, and eliminate the need for empirical inter-phasial transports.

This paper represents an initial step toward DNS of interfacially active multiphase flows. We report two-dimensional simulations of the sedimentation of solid particles in a hotter or colder fluid. Coupling fluid flow with heat transfer, this problem seems to be the simplest to contain the two mesoscopic features discussed above. The rest of the paper is organized as follows. Section 2 formulates the problem and discusses

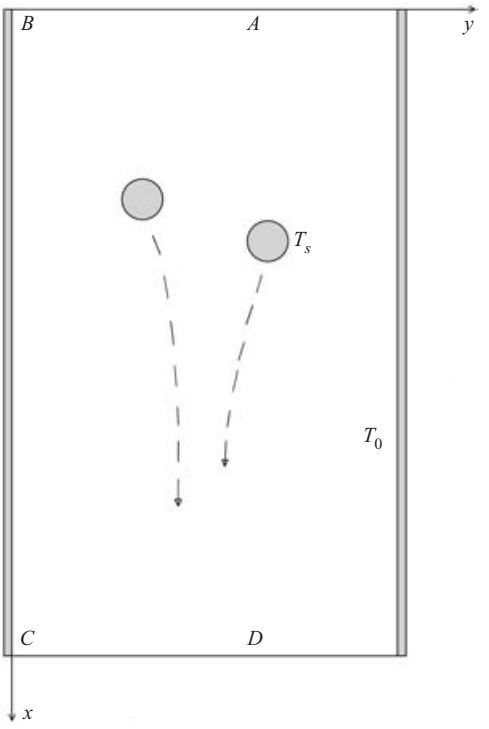

FIGURE 1. Schematic of the computational domain. The vertical channel has a width of W and is sufficiently long that the particles are little influenced by the position of the top and the bottom. The initial fluid temperature is T_0 and the solid temperature is fixed at T_s.

the theoretical model and numerical methods. Section 3 describes validation of the numerical scheme using test problems. Section 4 discusses the sedimentation of a single particle, and § 5 is devoted to the interaction between two particles. Conclusions are drawn in § 6.

2. Problem formulation and numerical methods

We release solid particles with zero initial velocity in a vertical channel filled with a Newtonian fluid (figure 1). In two dimensions, the particles are circles. The fluid has a uniform initial temperature T_0, and the solid is at temperature T_s. The particles start to settle under gravity and interact with each other and with the channel walls. We assume that the particle temperature remains uniform and fixed at T_s during the sedimentation. As is well known, transient heating of the particles is an appreciable effect if the thermal conductivity of the solid is not very large (Sirignano 1999). Though important in certain applications, it is not our main interest here. Besides, if we allow the solid temperature to vary, it will soon attain the fluid temperature and all thermal effects will vanish. Hence, a fixed T_s is a convenient device to simulate the long-time effects of thermal convection, which in reality may be sustained, say, by chemical reaction. Our rationale is to use this simplified problem to elucidate the basic physical mechanisms that are likely to be relevant to more general interfacially active two-phase flows. By the same token, the parameters used in the simulations are not intended to represent a particular material or process.

The continuity, momentum and energy equations for the fluid are

$$\nabla \cdot \boldsymbol{v} = 0, \tag{1}$$

$$\rho_0 \left(\frac{\partial \boldsymbol{v}}{\partial t} + \boldsymbol{v} \cdot \nabla \boldsymbol{v} \right) = -\nabla p + \mu \nabla^2 \boldsymbol{v} + \rho \boldsymbol{g}, \tag{2}$$

$$\rho_0 c_p \left(\frac{\partial T}{\partial t} + \boldsymbol{v} \cdot \nabla T \right) = k \nabla^2 T. \tag{3}$$

In equation (2), we use the Boussinesq approximation such that a temperature change only modifies the fluid density ρ in the body force term:

$$\rho = \rho_0 [1 - \beta (T - T_0)], \tag{4}$$

where ρ_0 is the fluid density at the far-field temperature T_0, and β is the coefficient of thermal expansion for the fluid. In equation (3), we have neglected viscous dissipation since the Eckert number is typically small in our simulations (cf. White 1991, p. 84). The ith particle translates and rotates according to the following equations:

$$m_i \frac{\mathrm{d}\boldsymbol{V}_i}{\mathrm{d}t} = \boldsymbol{G}_i + \boldsymbol{F}_i, \tag{5}$$

$$I_i \frac{\mathrm{d}\boldsymbol{\Omega}_i}{\mathrm{d}t} = \boldsymbol{T}_i, \tag{6}$$

where m_i and I_i are the mass and moment of inertia of the particle, $\boldsymbol{V}_i$ and $\boldsymbol{\Omega}_i$ are its velocity and angular velocity, and $\boldsymbol{G}_i$, $\boldsymbol{F}_i$ and $\boldsymbol{T}_i$ are the body force, hydrodynamic force and moment, respectively.

The motion of the particles and the fluid flow are coupled via the hydrodynamic force and moment and boundary conditions on the particle surfaces. We impose continuity of velocity (no-slip) and temperature on the particles. On the four sides of the computational domain we impose the following conditions (see figure 1):

$$\boldsymbol{v} = \boldsymbol{0}, \qquad T = T_0 \qquad \text{on} \qquad BC, CD \text{ and } DA;$$
$$\tau_{xy} = \tau_{xx} = 0, \qquad \frac{\partial T}{\partial x} = 0 \qquad \text{on} \qquad AB,$$

where τ represents total stress components. The top (AB) is drawn at a fixed distance above the trailing particle and the bottom (CD) at a fixed distance below the leading particle. Thus, the computational domain is redefined at each time step according to the positions of the particles, though the governing equations are solved in a fixed laboratory coordinate system. Therefore, $\boldsymbol{v} = \boldsymbol{0}$ on CD implies that the channel is so deep that the falling particles drive no net flow rate. At the top, downward flow in the wake of the particles is compensated by upward backflow; the stress-free conditions allow for a developing wake. The zero-heat-flux condition at an outflow section is often used in the literature but not always justifiable. For natural convection around a fixed hot particle (Sadeghipour & Razi 2001), for instance, the backflow carries fluid into the domain where the temperature would depend, in reality, on conditions outside the domain. This is, of course, not captured by the zero-heat-flux condition. This is not a serious concern in our sedimentation simulations since the computationa domain travels with the particles and there is usually no information being transported into the domain from outside AB.

To make the equations and boundary conditions dimensionless, we use the diameter of the particle d as the characteristic length. The characteristic velocity, denoted by

U, is to be specified later for different problems. The characteristic time is then d/U. We absorb the hydrostatic pressure due to $\rho_0 \boldsymbol{g}$ into the pressure gradient, and scale the 'dynamic pressure' by $\mu U/d$. The dimensionless temperature is defined as $(T-T_0)/|T_s-T_0| = (T-T_0)/\Delta T$. The force and torque on the two-dimensional particle are scaled by μU and $\mu U d$, respectively. Using the same symbols for the dimensionless quantities, we re-write the governing equations as

$$\nabla \cdot \boldsymbol{v} = 0, \tag{7}$$

$$Re\left(\frac{\partial \boldsymbol{v}}{\partial t} + \boldsymbol{v}\cdot\nabla\boldsymbol{v}\right) = -\nabla p + \nabla^2 \boldsymbol{v} - \frac{Gr}{Re} T \hat{\boldsymbol{i}}, \tag{8}$$

$$\left(\frac{\partial T}{\partial t} + \boldsymbol{v}\cdot\nabla T\right) = \frac{1}{RePr}\nabla^2 T, \tag{9}$$

$$\frac{\pi}{4}\frac{\rho_s}{\rho_0} Re \frac{\mathrm{d}\boldsymbol{V}_i}{\mathrm{d}t} = \boldsymbol{G}_i + \boldsymbol{F}_i, \tag{10}$$

$$\frac{\pi}{32}\frac{\rho_s}{\rho_0} Re \frac{\mathrm{d}\boldsymbol{\Omega}_i}{\mathrm{d}t} = \boldsymbol{T}_i, \tag{11}$$

where $\hat{\boldsymbol{i}}$ is the unit vector along the x-axis, and m_i and I_i have been replaced by $\pi\rho_s d^2/4$ and $\pi\rho_s d^4/32$, respectively. $\boldsymbol{F}_i$ is computed using the dynamic pressure, and $\boldsymbol{G}_i$ includes the buoyancy force due to $\rho_0 \boldsymbol{g}$. The dimensionless parameters are

$$\text{Reynolds number:} \quad Re = \frac{\rho_0 U d}{\mu},$$

$$\text{Grashof number:} \quad Gr = \frac{\rho_0^2 \beta \Delta T d^3 g}{\mu^2},$$

$$\text{Prandtl number:} \quad Pr = \frac{\mu c_p}{k}.$$

In presenting the results, we will occasionally refer to the Rayleigh number $Ra = GrPr$ as well.

We use a finite-element method to solve the coupled equations for the fluid and solid phases. The algorithm is based on an Arbitrary Lagrangian–Eulerian (ALE) technique developed for tracking moving particles in isothermal fluid–solid systems (Hu, Joseph & Crochet 1992; Feng, Hu & Joseph 1994); the only augmentation is for the energy equation. Details of the method can be found in a recent review by Hu, Patankar & Zhu (2001), and we will mention only a few salient features. We use an unstructured mesh of triangular elements generated by the Delaunay–Voronoi method. As the particles move, the mesh moves and deforms according to a 'mesh velocity' determined by a Laplace equation. When the elements become severely distorted, a re-meshing and projection procedure is carried out to restore mesh quality. When a particle approaches another particle or a wall, the local mesh is automatically refined. Collision is modelled via a 'contact force' that prevents two solid surfaces from touching. The governing equations are discretized using a Galerkin formulation; residues from the solid and fluid momentum equations are combined into one weak form. This way, the hydrodynamic force and moment cancel out between the two phases and need not be computed explicitly. The position of the particles is updated explicitly but their velocity is determined implicitly along with the fluid velocity to ensure stability of the scheme. The time step is automatically adjusted according to the velocity and acceleration of the particles. The nonlinearity in convection is handled

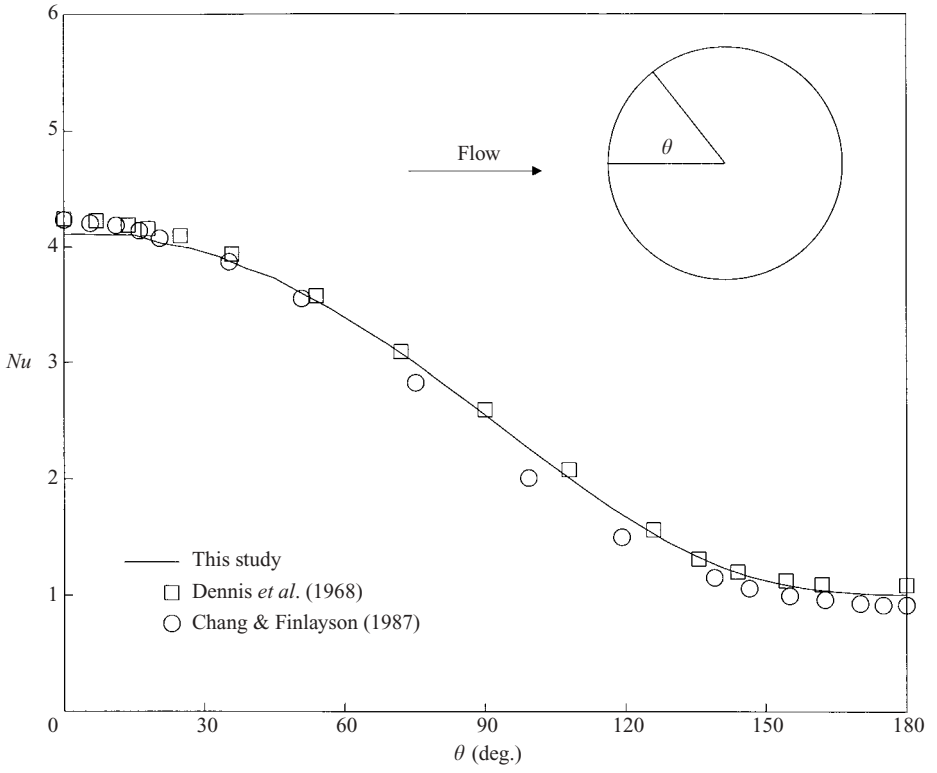

FIGURE 2. The local Nusselt number Nu on a cylinder subject to forced convection at $Re = 20$. The Reynolds number is defined using the far-field uniform velocity and the cylinder diameter.

by a Newton iteration and the linear systems are solved using iterative methods such as the preconditioned GMRES algorithm.

We should mention that our finite-element ALE 'particle mover' is one of several DNS methods that have emerged for two-phase flows in the past decade. Among others, Unverdi & Tryggvason (1992) developed a front-tracking method for drops and bubbles on a fixed grid and Ladd (1997) and Aidun & Lu (1998) used the Lattice–Boltzmann method to simulate a large number of solid particles in dense suspensions.

3. Test problems

The objective of this section is to validate our numerical scheme by solving problems with well-established solutions in the literature. We have chosen two test problems: forced convection around a cylinder in a channel and natural convection in the annulus between two horizontal concentric cylinders.

3.1. *Forced convection around a circular cylinder*

Chang & Finlayson (1987) computed the heat transfer from a circular cylinder placed in a steady uniform flow. We solved the same problem using the same geometry and parameters, and figure 2 compares the local Nusselt number Nu on the cylinder. Additional results by Dennis, Hudson & Smith (1968), using slightly different conditions on the outer boundary, are also shown. All three are in fairly close

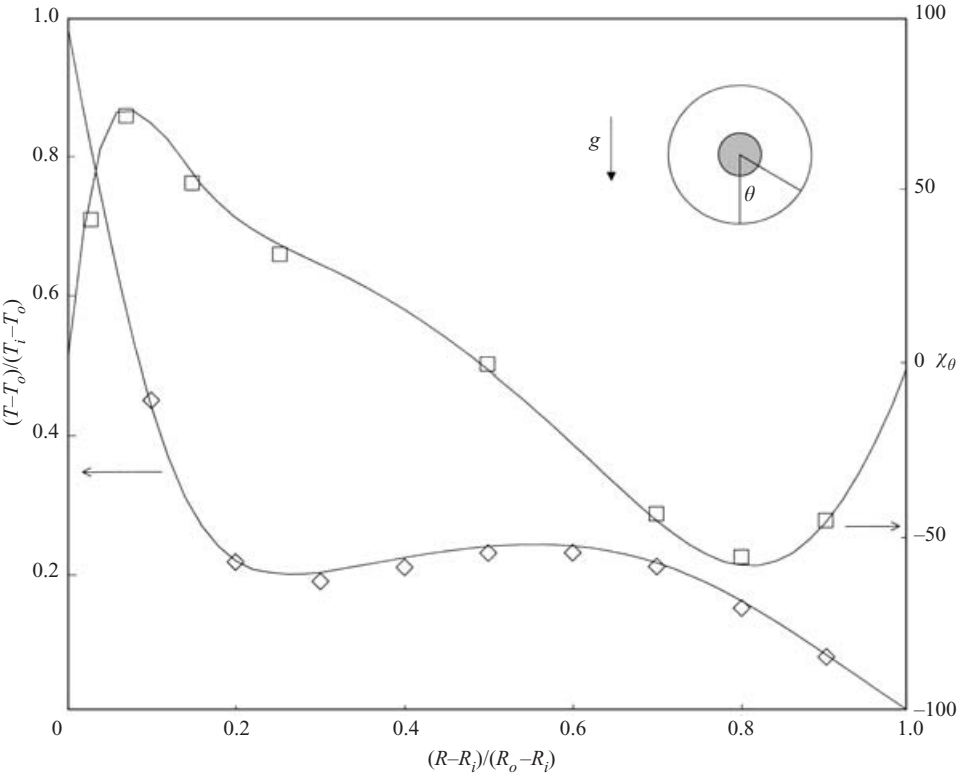

FIGURE 3. Radial temperature and velocity profiles along $\theta = 60°$ in an annulus between two horizontal concentric cylinders. The data points are from Kuehn & Goldstein (1976) and the solid lines are our results. The azimuthal velocity v_θ is made dimensionless by the gap size $(R_o - R_i)$ and the thermal diffusivity α.

agreement, though Chang & Finlayson's Nu is somewhat smaller at the side (near $\theta = 90°$). We performed extensive mesh refinement to ensure convergence. Our typical mesh giving acceptable accuracy is finer than the mesh used in Chang & Finlayson, and that is possibly the cause of the discrepancy.

3.2. *Natural convection between concentric cylinders*

To test our code's ability to handle natural convection, we simulated natural convection in the annulus between two horizontal concentric cylinders. The inner cylinder has a radius R_i and temperature T_i, while the outer cylinder has R_o and T_o. Kuehn & Goldstein (1976) studied this problem with the following parameters: $R_o/R_i = 2.6$, $Pr = 0.7$ and $Ra = 5 \times 10^4$, where the Rayleigh number Ra is defined using the gap width $R_o - R_i$. Figure 3 compares the radial temperature and velocity profiles from Kuehn & Goldstein (1976) and our calculations. The agreement is excellent. Based on the two test problems, we are confident that our code handles convective heat transfer accurately.

4. Sedimentation of a single particle

The sedimentation of a hot or cold particle in a fluid involves a combination of natural and forced convection. To investigate the various factors at play, we have

simulated three scenarios of sedimentation: (*a*) sedimentation with no thermal effect; (*b*) a cold particle settling in a hot fluid; (*c*) a hot particle settling in a cold fluid. Case (*a*) occurs when the fluid and solid have the same temperature, and will be referred to as the isothermal case. In analysing the results, we will often refer to the upward flow of the fluid relative to the particle as 'external flow'.

A circular particle of diameter d is released from the centreline, with zero initial velocity, in a channel of width W (cf. figure 1). The computational domain moves with the particle, its top and bottom being $15d$ and $10d$ from the particle centre. Numerical experiments have confirmed that the domain is long enough for the results to be insensitive to the position of the top and bottom. Mesh refinement has been performed to ensure convergence of the results, especially adequate resolution of the thermal and momentum boundary layers. The Prandtl number is fixed at $Pr = 0.7$. Unless otherwise specified, the characteristic velocity is the terminal velocity of the particle or the mean settling velocity for oscillatory solutions. This defines Re and the time scale.

4.1. *Isothermal sedimentation*

The sedimentation of a circular particle in a channel without thermal effects has been discussed by Feng *et al.* (1994) in great detail. Four regimes of particle behaviour have been identified for increasing Reynolds numbers. The threshold Re values between the regimes depend on the blockage ratio d/W. At low Re, steady sedimentation along the centreline of the channel is stable. At higher Re, the particle executes weak and somewhat irregular lateral oscillations about the centreline while settling. At still higher Re, the particle oscillates regularly with a large amplitude. The average lateral position is off the centreline except for strong wall confinement. Finally, for even higher Re, the oscillation becomes irregular. The regimes can be explained in terms of the dynamics of the wake and wall repulsion.

4.2. *Cold particle*

Depending on the Grashof number, a rich array of dynamics is observed for a cold particle settling with thermal convection. Five regimes have been delineated for Gr up to 10^4. The critical Grashof numbers are estimated from simulations in the neighbouring regimes. Most of the simulations presented here are for a solid-to-fluid density ratio $\rho_s/\rho_0 = 1.00232$ in a channel of width $W = 4d$. We will also refer to results in a wider channel in examining the effects of wall confinement. As a baseline, an isothermal particle of the same density settles steadily along the centreline of a $4d$ channel at $Re = 21.0$.

Regime A ($0 < Gr < 500$)

In this regime, the only effect of the downward convection is to increase the final settling speed, and the effect is stronger at higher Gr (figure 4). The particle accelerates monotonically after release, and eventually settles steadily along the centreline (figure 5). In a reference frame fixed on the particle, the flow and temperature fields are steady and symmetric, with a pair of standing vortices behind the particle.

Regime B ($500 < Gr < 810$)

In this regime, the particle develops a regular lateral oscillation (figure 5*b*). The average position also moves slightly away from centreline, and the particle rotates with a small oscillating angular velocity. The vertical velocity u increases monotonically at the beginning and eventually settles into a small-amplitude oscillation about a constant value. The amplitude is so small at $Gr = 564$ as to be nearly invisible in figure 5(*a*).

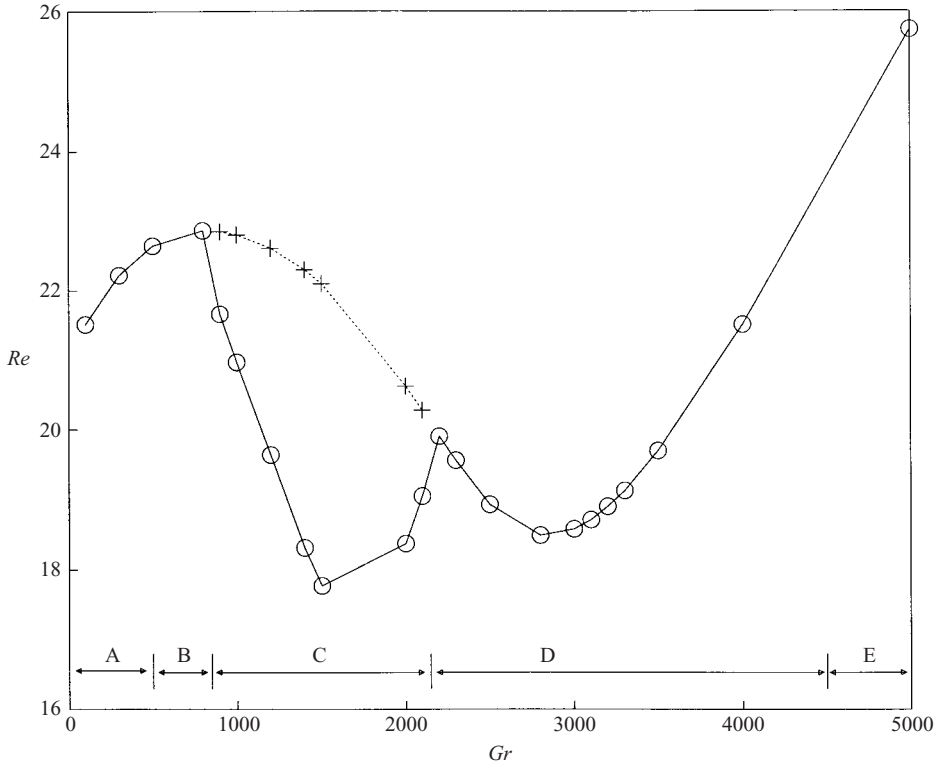

FIGURE 4. Terminal velocity U, indicated by the Reynolds number Re, of a cold particle in various Gr-regimes. U is the mean for oscillatory solutions in Regimes B and E. The + symbols and dotted line represent the settling velocity on the centreline before the particle migrates sideways in Regime C.

The oscillatory behaviour is similar to that observed for an isothermal particle at higher Re (Feng *et al.* 1994). The cause of the oscillation also turns out to be the same: vortex shedding from the particle. This is confirmed by studying the flow field in figure 6. Without thermal convection, regular vortex shedding in a $W = 4d$ channel does not occur until $Re \approx 70$ (Feng *et al.* 1994). In the present case, the tendency of the cold fluid layer next to the particle to sink counters the upward momentum of the external flow. This precipitates vortex shedding and oscillation of the wake, which would be symmetric and steady otherwise. A telltale sign of the downward convection is the local maxima of vorticity at the back of the particle (figure 6*b*). These maxima are more pronounced than in Regime A.

The deviation of the average lateral position from the centre of the channel increases with Gr but remains small in this regime, being $0.09d$ for $Gr = 800$, for example. The amplitude of lateral oscillation appears to increase with Gr.

Regime C ($810 < Gr < 2150$)

In this regime, the particle eventually achieves steady-state settling close to one of the walls. The approach to this final state depends on Gr. For lower Gr values, the particle's behaviour is a natural extension of Regime B. It oscillates while gradually migrating away from the centreline. As the particle nears the end of its migration, the oscillation slowly dies out to give way to steady sedimentation (e.g. $Gr = 850$

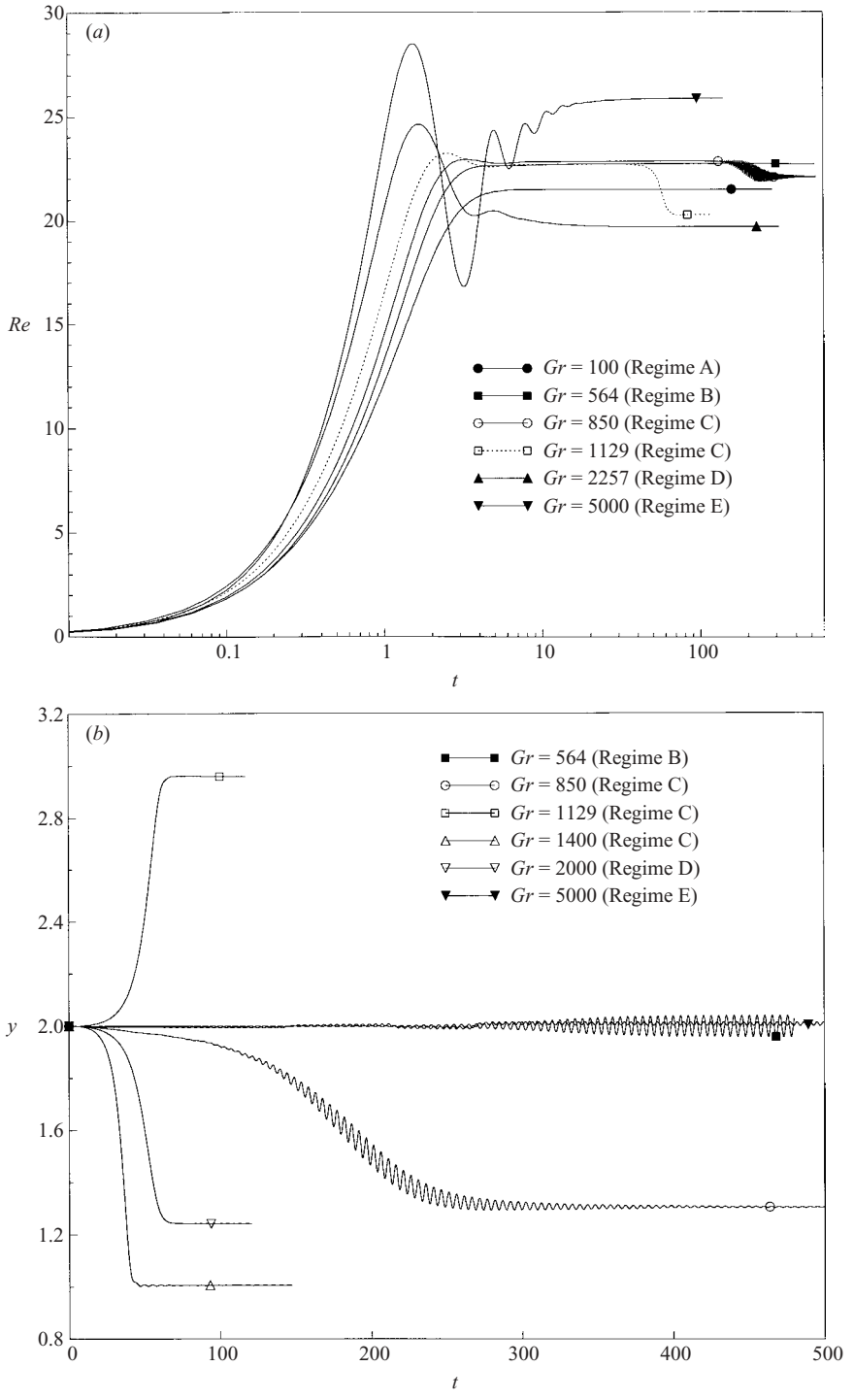

FIGURE 5. Transients for the sedimentation of a cold particle at Grashof numbers representing the five regimes. (*a*) The settling velocity $u(t)$ represented by the instantaneous Reynolds number $Re(t)$; (*b*) the lateral position y scaled by d. For Regimes A and D, the particle stays on the centreline ($y = 2$) and the trajectories are omitted for clarity. In both plots, t is scaled by d/U, U being the terminal velocity.

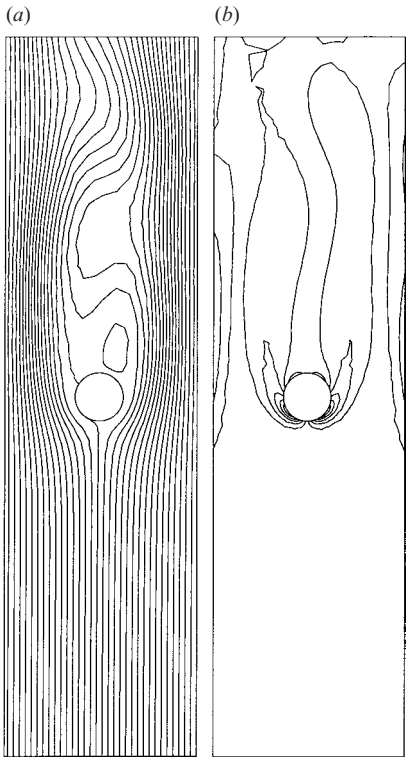

FIGURE 6. Snapshots of the flow field around a cold particle in Regime B ($Gr = 564$) at $t = 377.5$. (a) Streamlines in a reference frame fixed on the particle. Vortex shedding is phase-locked with the particle's oscillation; (b) vorticity contours.

in figure 5b). For higher Gr in this regime, oscillation never appears. The particle simply migrates off the centreline to an off-centre equilibrium position (e.g. $Gr = 1129$ in figure 5b). In both cases, the settling velocity has an initial overshoot and then apparently stabilizes (figure 5a). A further drop in u accompanies the lateral migration, evidently as a result of wall proximity. As soon as it deviates from the centreline, the particle acquires a rotation in the 'normal' sense, i.e. as if rolling down the nearer wall (Liu *et al.* 1993).

This regime has two remarkable features: suppression of vortex shedding and destabilization of sedimentation along the centreline. The former is due to wall confinement. The downward thermal convection collides with the upward external flow in the boundary layer, causing separation to occur farther upstream and generating a wider and longer wake (figure 7). A wide vortex street is apparently not permitted if the channel is too narrow. This is supported by simulations in a wider channel of width $W = 8d$, where vortex shedding persists through all higher-Gr regimes.

The lateral migration is a surprising manifestation of the conflict between the downward thermal convection and upward external flow. The downward flow impinges on the back of the particle (figure 7a), creating a high pressure at the back stagnation point. Also note the two maxima of vorticity at the back, which are almost as pronounced as those on the front side due to the external flow (figure 7b). The counterbalance between the high pressures at the front and the back sets up

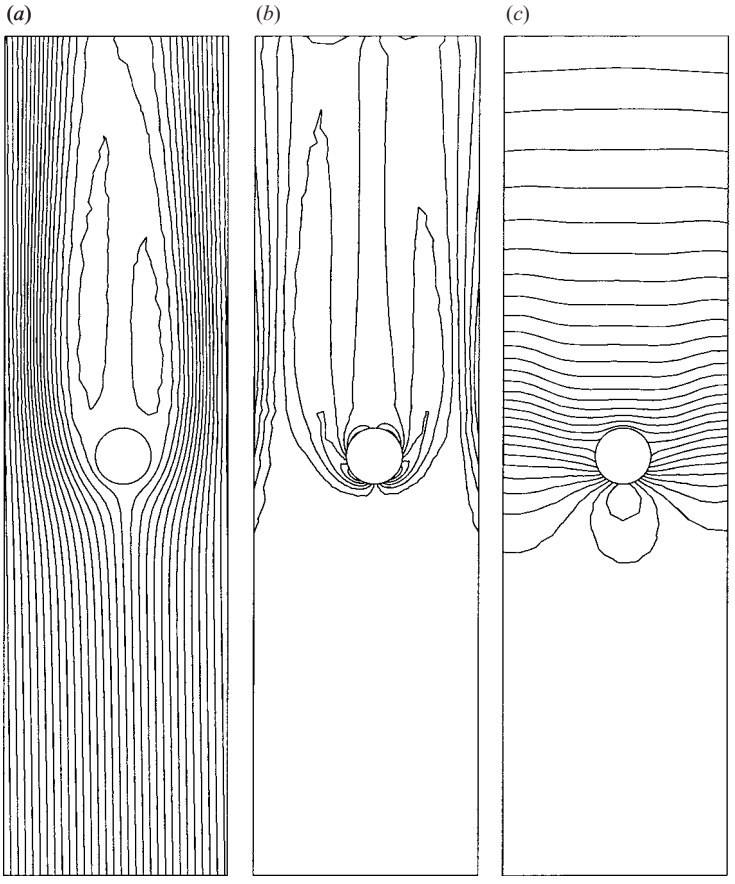

FIGURE 7. Flow and pressure fields around a cold particle in Regime C ($Gr = 1129$) at $t = 40.39$, when the particle has just started to migrate to the right. (a) Streamlines in a reference frame fixed on the particle – vortex shedding is suppressed; (b) vorticity contours; (c) asymmetric pressure contours with higher p on the left side of the particle.

a 'buckling instability'. If a lateral disturbance displaces the particle slightly to the right, say, both the up- and down-flows would tend to go around the particle's left side. This shifts the front and back stagnation points toward the left, resulting in an asymmetry in the pressure field and a lateral force that further pushes the particle to the right (figure 7c). Thus, settling along the centreline is destabilized.

As Gr increases from 810 to 1400, the equilibrium position shifts toward the wall and the terminal velocity decreases (figures 4, 5). The migration also onsets sooner after release and takes shorter time for higher Gr. For Gr between 1400 and 1500, the particle centre is roughly midway between the centre of the channel and the wall. As Gr increases beyond 1500, however, the trend is reversed. The equilibrium position shifts back toward the centre, the terminal velocity increases and the migration takes longer. We believe the reversal is caused by increased wall repulsion, which eventually leads to a dramatic re-stabilization of the centreline in the next regime.

Regime D ($2150 < Gr < 4500$)

In this regime, the centreline becomes once again a stable equilibrium position. The fall velocity has a large initial overshoot before approaching a terminal value

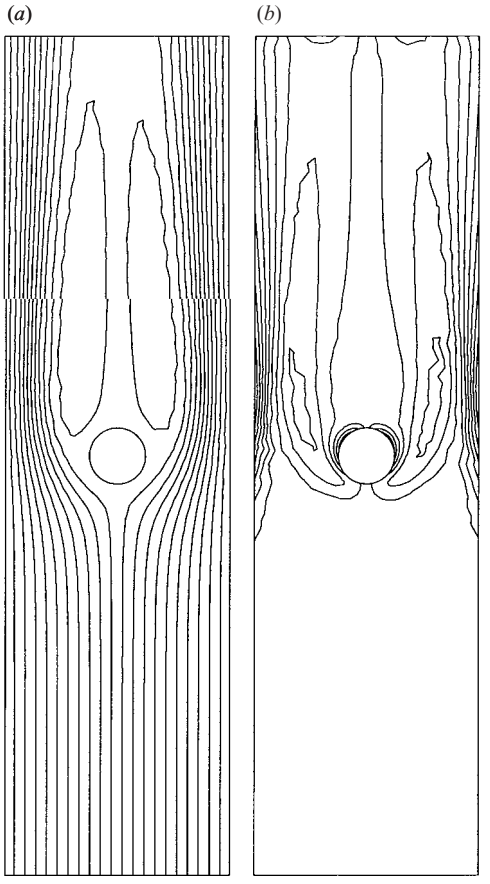

FIGURE 8. Snapshots of the flow field around a cold particle in Regime D ($Gr = 2257$) at $t = 65.35$. (*a*) Streamlines in a reference frame fixed on the particle; (*b*) vorticity contours.

(figure 5*a*). Vortex shedding is still absent, and the flow field is symmetric and steady in a reference frame fixed on the particle (figure 8). The downward convection is stronger and dominates the area surrounding the particle. The vorticity maxima at the front have nearly disappeared and those on the back move forward. The rear stagnation point supersedes the front stagnation point as the location of maximum heat transfer.

The re-stabilization of sedimentation along the centreline is the culmination of the gradual shift of the equilibrium position toward the centre in the previous regime. The cause of this process seems to be related to the strong wall confinement. Figure 8 illustrates how the strong downward convection impinges on the back of the particle and creates a wake that occupies more than half of the channel width. The upward stream splits in front of the particle into two branches, each having a strong lateral component toward the walls. This raises the lateral pressure gradient on the two sides, creating a stronger wall repulsion which inhibits deviation from the centreline. Heuristically, the thermal convection makes the particle appear larger to the external flow, causing the stronger wall confinement.

The terminal velocity does not change monotonically with Gr in this regime; it decreases from $Gr = 2200$ to 2800, and then increases with increasing Gr even into

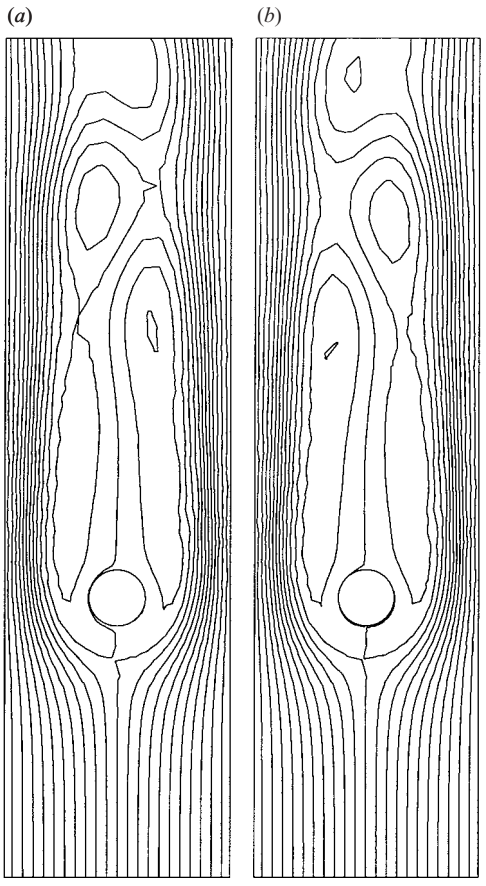

FIGURE 9. Kelvin–Helmholtz instability in the shear layers downstream of a cold particle in Regime E ($Gr = 5000$). (a) Streamlines at $t = 230.7$ with vortex roll-up on the left; (b) streamlines at $t = 232.6$ with vortex roll-up on the right.

the next regime (figure 4). This is related, perhaps, to the fact that on the one hand the downward convection impinges on the back of the particle and enhances U, while on the other it causes a wide wake which gives the particle a higher drag coefficient. The competition between the two mechanisms reduces U at lower Gr but does the opposite at higher Gr.

Regime E ($Gr > 4500$)

The final regime is characterized by the re-emergence of lateral oscillations about the centreline (figure 5b). The amplitude is small – a little over 1% of the particle diameter at $Gr = 5000$ – but grows with Gr. The settling velocity overshoots and undershoots several times, eventually stabilizing at a terminal value that increases with Gr (figures 4, 5a). The lateral oscillation becomes somewhat irregular at $Gr = 10^4$, and the amplitude seems to be modulated between $0.2d$ and $2d$.

The oscillation of the particle is reminiscent of Regime B, but vortex shedding is completely absent here. The thermal convection is so strong as to engulf the particle entirely. It then collides with the up-flow and creates a stagnation point ahead of the particle (figure 9). This generates a very long and wide wake, which oscillates, due apparently to a Kelvin–Helmholtz instability of the shear layers. Figure 9 shows two

snapshots of the wake when the shear layers roll up far downstream to form a vortex on the left and right. These are also times when the particle is the farthest to the left and right, respectively. Therefore, the oscillation of the particle is phase-locked with the roll-up of shear layers in the wake due to Kelvin–Helmholtz instability. Since the roll-up occurs far downstream of the particle, the periodic forcing is weak, and the amplitude of the particle's oscillation is small. The frequency of oscillation corresponds to a Strouhal number of 0.173, somewhat lower than the value of 0.199 for $Gr = 564$. At higher Gr, the oscillation in the wake becomes stronger but less regular, still phase-locked with the motion of the particle.

To explore the effects of wall confinement, we carried out simulations in a wider channel ($W = 8d$). Steady settling along the centreline (Regime A) prevails up to $Gr = 3000$. Once vortex shedding occurs, it is never suppressed at higher Gr. Thus, Regimes B and C are combined into one; the particle migrates off the centre, and oscillates laterally about a near-wall equilibrium position while settling. With increasing Gr, the equilibrium position moves first toward the wall, and then back to the centre. Regime D disappears and Regime E prevails at higher Gr, with the particle oscillating about the centreline while settling. The cause of the oscillation is still vortex shedding, off the sides or even the front of the particle because of the strong downward convection. This produces a wide wake.

To summarize, the sedimentation of a cold particle exhibits complex dynamics in which two factors are at play. The first is the competition between the upward external flow and the downward thermal convection in areas surrounding the particle. The second is wall effects. The first is responsible for increasing the settling speed in Regime A, precipitating vortex shedding in Regime B and destabilizing the centreline in Regime C. It also generates a wide wake which is more susceptible to wall effects. Thus, the two factors conspire in restabilizing the centreline in Regime D and finally causing shear-layer roll-up in Regime E. Regardless of the regimes, the particle always attains a higher initial velocity for larger Gr (figure 5*a*). This reflects the immediate effect of a downward convection striking the back of the particle. Later, the flow field farther away from the particle is established, and the fall velocity is adjusted accordingly. The terminal velocity varies with Gr in a complex way (figure 4).

4.3. *Hot particle*

For a hot particle settling in a cold fluid, natural and forced convection are in the same direction. This to some degree simplifies the dynamics. Three regimes have been identified. All parameter values are the same as for the cold particle except where noted otherwise.

Regime A ($0 < Gr < 500$)

The fall velocity may undergo an initial overshoot (figure 10). Eventually the particle settles steadily along the centreline; the terminal velocity decreases with Gr as one expects. Thermal convection does modify the flow field in one key aspect: boundary layer separation is suppressed if Gr is not too small, and no vortices trail the particle. The hot layer of fluid next to the particle carries upward momentum, and survives the adverse pressure gradient on the downstream side of the particle without detaching from the solid surface. The effect is similar to the suppression of boundary-layer separation by blowing downstream (Schlichting 1979), and it operates throughout the higher-Gr regimes to be discussed next. Another notable feature is the appearance of a 'negative wake' some distance behind the particle, where the flow

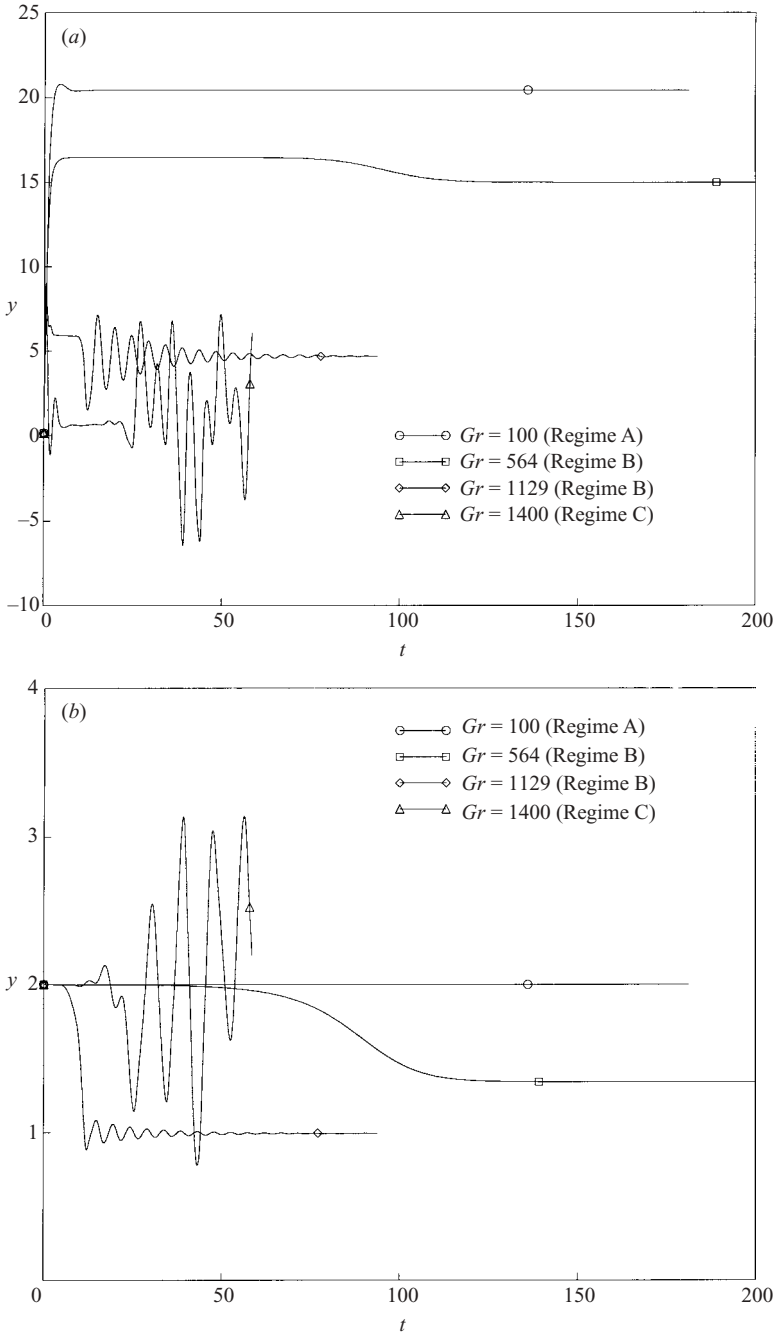

FIGURE 10. Sedimentation of a hot particle in three *Gr*-regimes. (*a*) The instantaneous Reynolds number $Re(t)$; (*b*) the lateral position y. In scaling t, the characteristic velocity is taken to be the terminal velocity for Regimes A and B, and the maximum velocity for Regime C.

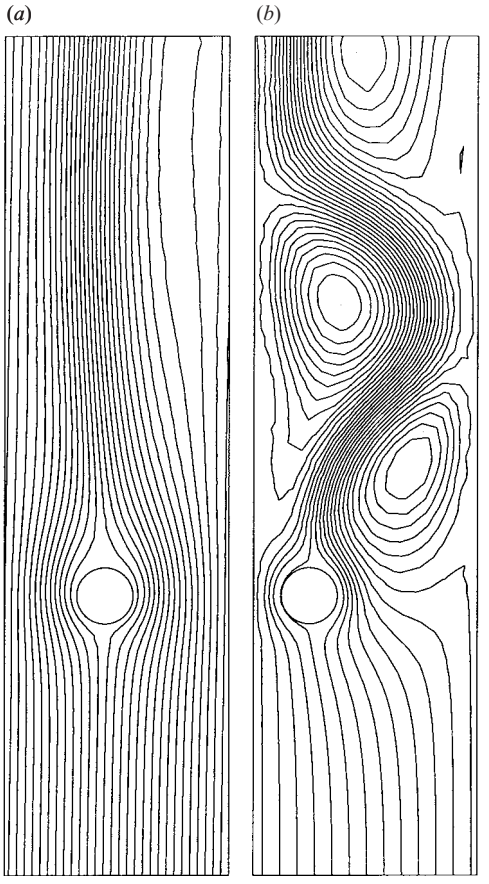

FIGURE 11. (*a*) Streamlines past a hot particle in Regime B ($Gr = 564$) at $t = 80.25$. The hot plume behind the particle bends toward the left wall and the asymmetry drives the particle to the left. (*b*) Streamlines showing the stationary serpentine wave behind a hot particle that settles steadily close to the left wall. $Gr = 1129$.

is upward with respective to the channel walls. This feature becomes stronger with increasing Gr and persists in the following regimes as well.

Regime B ($500 < Gr < 1250$)

At first sight, this regime resembles Regime C for the cold particle. Soon after release, the particle starts to migrate off the centreline, eventually achieving an asymmetric equilibrium position. For Gr values close to the lower bound of this regime, the approach to the final equilibrium position is smooth and monotonic (e.g. $Gr = 564$ in figure 10*b*). For higher Gr, the particle undergoes a damped oscillation before stabilizing at its off-centre equilibrium position (e.g. $Gr = 1129$ in figure 10*b*). For slightly heavier particles ($\rho_s/\rho_0 = 1.00310$), we also found a narrow range of Gr in which the small-amplitude oscillation does not die out. Once the particle is off the centre, it rotates anomalously, i.e. as if rolling up the nearby wall. With increasing Gr, the equilibrium position first moves toward the wall and then back toward the centreline, a phenomenon again mirroring Regime C of § 4.2.

However, the cause of the lateral migration is very different from that for the cold particle. Figure 11(*a*) shows the flow field for $Gr = 564$ at $t = 80.25$, when

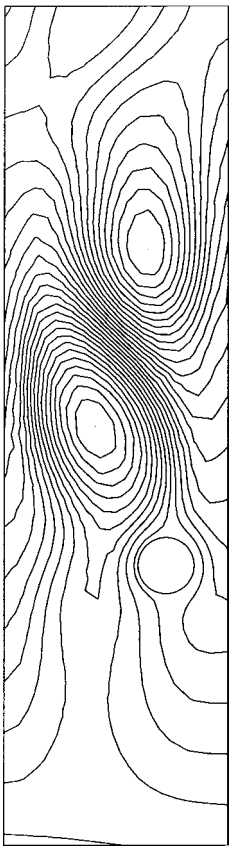

FIGURE 12. A snapshot of the flow field around a hot particle in Regime C ($Gr = 1400$) at $t = 46.81$. The reference frame is fixed on the particle whose lateral motion produces the artifact of streamlines intersecting the side walls.

the migration is well established. The warm wake forms a strong upward thermal plume. Such a plume is unstable because of the so-called Coanda effect (see e.g. Newman 1961). If the jet is displaced slightly to the left, say, the faster flow near the left wall will reduce the local pressure to further attract the jet. Thus the asymmetric flow pattern in figure 11 results. The lateral migration is driven by the high pressure on the right side as well as the strong shear stress on the upper right of the particle where the streamlines wrap around it. The latter explains the anomalous rotation of the particle.

For higher Gr in this regime, the hot plume is liable to another form of instability. This is the two-dimensional counterpart of the 'corkscrew' waves that Hu & Patankar (1995) analysed for a cylinder of lighter fluid surrounded by a denser fluid in a vertical pipe. As the particle deviates from the centreline, the plume starts to oscillate and assumes a serpentine shape (figure 11*b*). The oscillation is mild in that the shape of the plume barely changes; only the size of the vortices fluctuates. The period of the oscillation is typically much longer than that of vortex shedding in § 4.2. As the particle approaches its off-centre equilibrium position, the oscillation dies out and the plume settles into a stationary standing wave. Figure 11(*b*) depicts the final steady state for $Gr = 1129$. For slightly heavier particles ($\rho_s/\rho_0 = 1.00310$), we have also obtained solutions where the oscillation of the wake, and of the particle, persists

without damping. For sufficiently heavy particles, the fast external flow stabilizes the plume and the serpentine wave is completely suppressed.

As Gr increases, so does the lateral meander of the plume, and the vortices grow in size. This forces the particle to move away from the wall. Hence the equilibrium position shifts back toward the centreline as Gr approaches the upper bound of this regime.

Regime C ($Gr > 1250$)

In this regime, the particle executes a large-amplitude, low-frequency oscillation about the centreline (figure 10*b*). The vertical velocity oscillates as well and is frequently negative, i.e. upward (figure 10*a*). This regime appears to be a natural extension of the last one. The particle is pushed back to the centreline because the growing vortices demand more space. Once the particle is away from the wall, the plume gains the freedom to oscillate in time, swaying laterally with an amplitude much greater than is typical of the near-wall oscillation of the last regime. This causes the particle to oscillate both horizontally and vertically. Figure 12 shows a snapshot of the flow field at $t = 46.81$ for $Gr = 1400$.

To sum up this section, the dominant physical mechanism in the sedimentation of a particle with thermal effects is the competition between natural and forced convection. This determines the dynamics of the wake, and involves wall effects. As a result, isothermal, cold and hot particles behave quite differently in sedimentation.

5. Sedimentation of doublets

We will follow the structure of the last section by discussing, in sequence, particle interactions in the absence of thermal effects (isothermal particles) and with thermal convection for cold and hot particles. In the limiting cases of fast sedimentation, thermal convection will be overwhelmed and one expects the dynamics to revert to that of isothermal particles. The discussion below concerns moderate values of $Re = O(10)$ and Gr from 100 to a few thousand. The Prandtl number is fixed at $Pr = 0.7$ and the channel width at $W = 8d$. Note that the regimes for a single particle are often demarcated by the equilibrium position, which depends on the wall effect. For doublets, the wall effect is largely overshadowed by particle–particle interactions, and lateral migration is no longer a prominent feature. Hence, the behaviour of doublets will involve fewer regimes.

5.1. *Isothermal doublets*

Feng *et al.* (1994) have briefly discussed the interaction of isothermal doublets during sedimentation. Now a more complete picture is available. The most fundamental mechanism for doublet interaction is the drafting–kissing–tumbling (DKT) scenario first observed in experiments (Fortes, Joseph & Lundgren 1987). The trailing particle accelerates into the wake of the leader. When the two come near to contact, their line of centres rotates, with the trailing particle falling around the other and taking the lead. The process then repeats. The DKT scenario has many variants depending on the Reynolds number and wall proximity. At moderate Re, the process is periodic and regular (figure 13). As Re increases, the process occurs more rapidly and becomes 'quasi-periodic' with a degree of irregularity. Vortex shedding occurs at sufficiently high Re, producing oscillations at a higher frequency and smaller amplitude superimposed onto that due to the interaction of the particles. For decreasing Re, on the other hand, the interaction becomes slower and milder. Below a certain Re, the

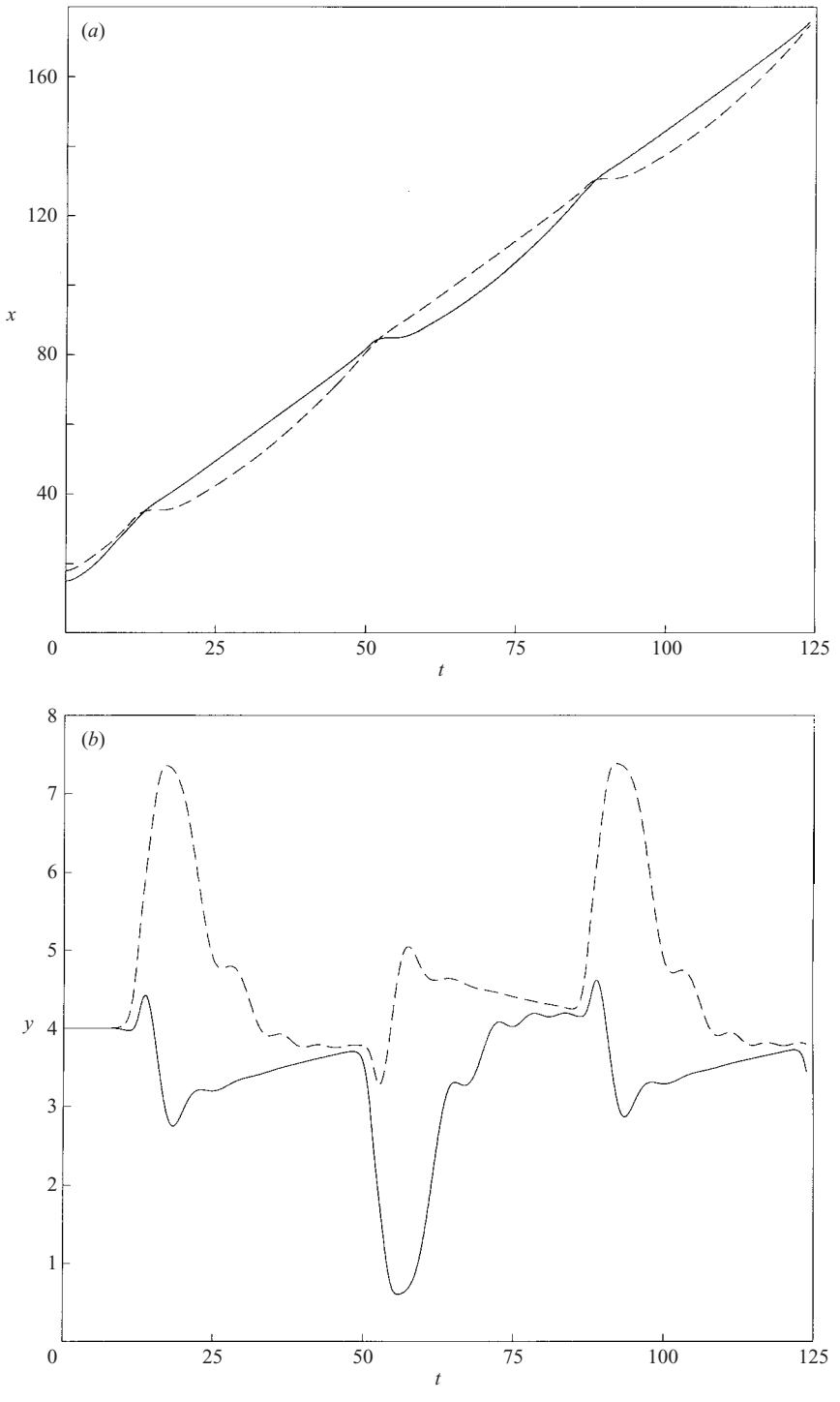

FIGURE 13. Trajectories for an isothermal doublet undergoing DKT cycles: (*a*) vertical position $x(t)$, (*b*) horizontal position $y(t)$. The centreline of the channel is at $y = 4$. $Re = 17$ based on the mean velocity, which is also used to scale t.

particles no longer exchange vertical position; the trailer catches up momentarily, and then swerves to the side and falls behind again. At lower *Re*, the two particles form a staggered structure and oscillate locally. At still lower *Re*, the amplitude of the oscillation goes to zero and a steady-state staggered solution obtains.

Wall confinement has two effects on doublet interaction. First, it intensifies interaction in the sense that the particles encounter each other more frequently in a narrower channel, and the process is faster. On the other hand, wall confinement is also stabilizing as it limits the freedom of lateral motion. Thus, in a narrower channel the particles are more likely to stay in a staggered structure, steady or oscillatory, and less likely to exchange vertical positions.

We have tested different initial configurations, with the two particles in tandem, staggered or abreast. The initial evolution of the solution is different but the long-time behaviour is the same. This is also true for the non-isothermal doublets discussed below.

5.2. *Cold doublets*

For cold particles, thermal convection affects particle–particle interactions mainly via the cold and heavy wake behind the leading particle. The most dramatic manifestation of this effect is the suppression of the DKT scenario at moderate *Gr*; figure 14 shows an example of this at $Gr = 141$. After release, the trailing particle is pulled toward the leader several times, but then the two separate and settle into a more or less fixed longitudinal separation of approximately $23d$. In the meantime, both oscillate laterally with the same frequency; the leader has a much smaller amplitude and leads the other slightly in phase. The two settle at a Reynolds number of $Re = 14.2$, at which two isothermal particle would execute the periodic DKT motion. Here, the trailing particle is settling in the cold and dense wake of the leading particle, and hence experiences a greater buoyancy force and produces a weaker downward convection in its own neighbourhood. Both effects oppose drafting, and a roughly constant vertical separation obtains as a result of the balance between the competing forces. Inspecting the flow field around the particles shows that the lateral oscillation is due to vortex shedding, an effect characteristic of Regime B of § 4.2. The trailing particle is forced by its own wake to the rear and by the wake of the leading particle in front. This causes a kind of resonance which explains the much larger amplitude for the trailer.

At higher *Gr*, the interaction is more vigorous and an example is shown in figure 15 for $Gr = 2200$. A mild form of DKT prevails for an initial period of time. As the trailer accelerates downward toward the leader, it is prevented from a close encounter by the strong convection stream which impinges on the back of the leader and diverges sideways (cf. figure 8). This diverging flow deflects the trailer, forcing it to go around the leader from a distance as if the leader had a much larger diameter. As the trailer overtakes the leader, the backflow due to the wake of the former temporarily drives the latter upward. A similar phenomenon is seen for an isothermal particle but the magnitude is much smaller. The cycle repeats until $t \approx 45$, when the two separate vertically to a more or less fixed distance and oscillate laterally. DKT is again suppressed. The lateral manoeuvre in figure 15(*b*) is due to particle interaction; vortex shedding has been eliminated by thermal convection in the same way as for a single cold particle (cf. Regime C of § 4.2). With increasing *Gr*, the initial DKT persists longer, and the final vertical separation decreases (from $23d$ at $Gr = 141$ to $19.5d$ at $Gr = 1200$ and $9.5d$ at $Gr = 2200$). There probably exists a threshold *Gr* above which DKT will not be suppressed, but we did not attempt to determine this value.

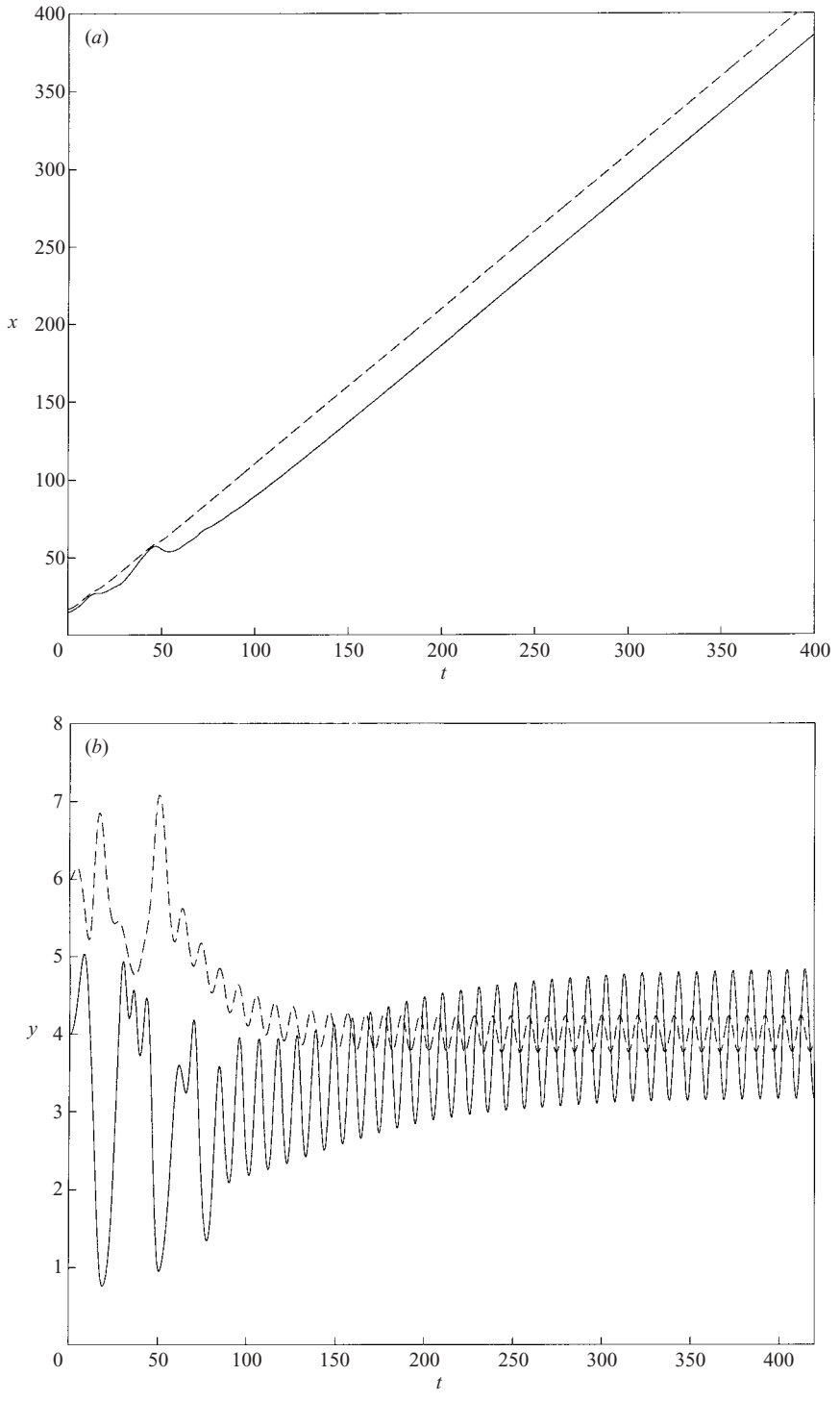

FIGURE 14. Suppression of DKT for a cold doublet settling at $Re = 14.2$ and $Gr = 141$: (*a*) vertical position $x(t)$; (*b*) horizontal position $y(t)$. The oscillation is due to vortex shedding.

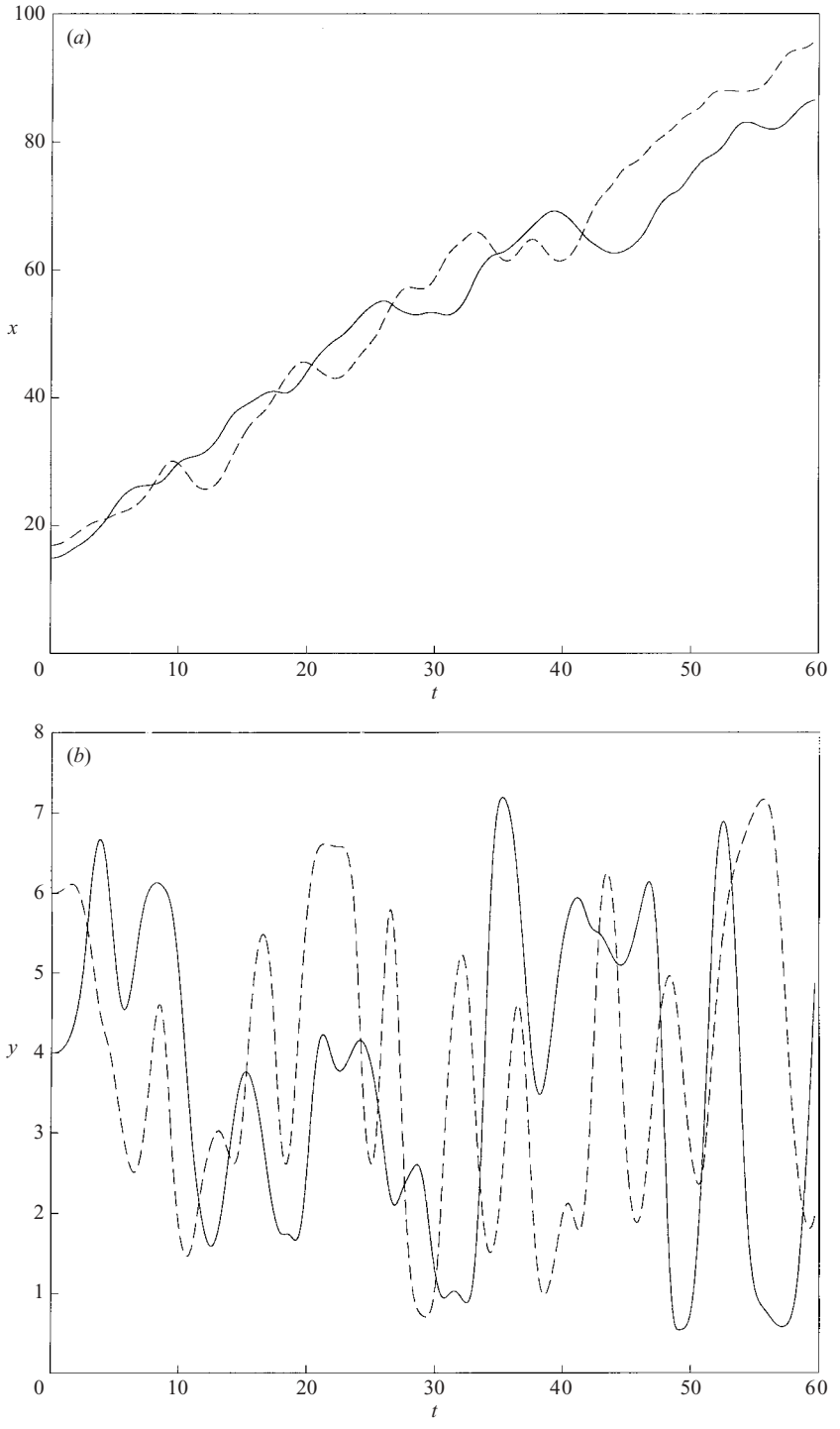

FIGURE 15. Trajectories of a cold doublet settling at $Re = 15$ and $Gr = 2200$. When one particle overtakes another, the latter is ejected upward and x dips. The two eventually separate vertically to a roughly constant distance apart.

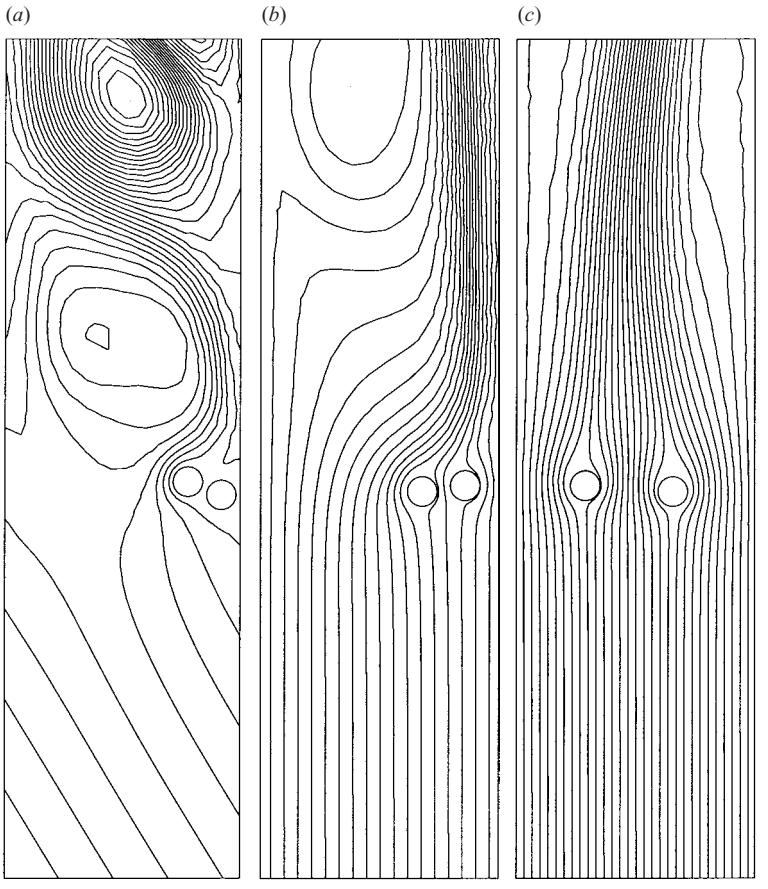

FIGURE 16. Streamlines around two hot particles at $Gr = 500$. (*a*) Solid–fluid density ratio $\rho_s/\rho_0 = 1.0170$ – the instantaneous $Re = 3.76$; (*b*) $\rho_s/\rho_0 = 1.0186$ – steady settling at $Re = 8.83$; (*c*) $\rho_s/\rho_0 = 1.0209$ – steady settling at $Re = 19.3$.

The foregoing discussion suggests that the main effect of thermal convection is to keep cold particles apart; their separations, both lateral and longitudinal, are greater than those for isothermal particles falling at a comparable *Re*. At smaller *Gr*, the cold wake repels a trailing particle through a larger buoyancy force. At larger *Gr*, the downward flow in the wake diverges upon impinging on the back of a particle and repels neighbouring particles. In a multi-particle system, these mechanisms will promote dispersion of cold particles and impede the formation of aggregates.

5.3. *Hot doublets*

In contrast to the cold doublet, a hot doublet tends to stay close thanks to thermal convection. The reason is that the rising plume in the wake draws fluid from neighbouring areas; the converging flow tends to attract nearby particles through 'entrainment'. This effect is suppressed for heavy particles, however, for which the fast external flow (i.e. forced convection) dominates the natural convection. In fact, the numerical results may be understood as a competition between natural convection (*Gr*) and forced convection (*Re*): at higher *Gr*, the particles tend to stick together and act as one, whereas at higher *Re*, they tend to separate.

Figure 16 compares three runs at $Gr = 500$ for different Re values achieved by varying the solid density. For the lightest particles (figure 16*a*), thermal convection causes the two to attract each other. They come to near contact and effectively form one elongated body. Note that the two approach each other sideways but one is not sucked into the other's wake, perhaps because the wake is warm and light. As is the case for a single hot particle (§ 4.3), the hot plume destabilizes, settling along the centreline of the channel. Thus, the doublet drifts toward a side wall (cf. figure 10*b* for a single hot particle). In this case the lateral migration is aided by the orientation of the effective long body. The plot shows the moment before the doublet collides with the wall, with an instantaneous $Re = 3.76$ based on the longitudinal velocity. Note also the serpentine thermal plume which resembles that for a single hot particle (figure 11*b*).

The heavier particles in figure 16(*b*) settle faster, and repel each other more in the way that two isothermal particles repel (Joseph *et al.* 1994). Hence, the two are farther apart. The solution approaches a steady state with the two settling side by side at a constant speed corresponding to $Re = 8.83$. In addition, the sinuous instability of the hot plume is suppressed by the fast external flow. This again is reminiscent of the behaviour of a single hot particle. With increasing Re, the two particles tend to separate more, with their centre of mass moving toward the centreline of the channel. The heaviest particles in figure 16(*c*) settle steadily at $Re = 19.3$, each on one side of the centreline. The trend shown in figure 16 prevails for Gr ranging from 100 to 1000, though for lower Gr values the sinuous instability of the thermal plume does not occur. We did not explore higher Gr values where the instability of the thermal plume may cause the particle to oscillate (cf. Regime C of § 4.3).

To sum up, the behaviour of a hot doublet is governed by the competition between natural and forced convection. As a rule, the thermal convection in the wake causes neighbouring particles to aggregate and behave as one, though the effect is diminished by external flow for heavier particles. In a settling suspension of hot particles, therefore, one may expect more pronounced aggregation than would appear for isothermal particles at the same Re (Fortes *et al.* 1987).

6. Conclusions

The general question that we set out to answer is how thermal convection affects the motion and interaction of particles in a two-phase system. Our numerical results indicate that thermal convection modifies the dynamics of sedimentation in a fundamental way. Within the parameter ranges examined, the following conclusions can be drawn:

(*a*) The sedimentation of a single particle is governed by the competition between natural and forced convection, which determines boundary layer separation, vortex shedding and the dynamics of the wake. These, coupled with wall effects, define a rich array of Gr-regimes for cold and hot particles.

(*b*) The interaction of particles is governed by the behaviour of the wake as influenced by thermal convection. Thus, cold particles tend to disperse and hot particles tend to aggregate.

(*c*) The microstructures in a sedimenting suspension of cold and hot particles are expected to be markedly different from those in the absence of thermal effects.

It is unfortunate that we have found little prior work, experimental or theoretical, with which to compare our results. Thus, in assessing the significance of our findings, we have to emphasize the simplifications and limitations contained in this work. First,

the simulations are two-dimensional. Comparison among prior two-dimensional and three-dimensional simulations of particulate flows, without thermal effects, shows that two-dimensional results capture the essential three-dimensional physics for smaller Reynolds numbers. As *Re* exceeds 100 or so, however, two-dimensional and three-dimensional dynamics become qualitatively different. The simulations reported here have *Re* well below that limit. Thus, we expect to find similar regimes in three-dimensions, though the critical parameter values will be different. Second, the setup of the problem and the parameter values are idealized and probably unrealistic. For instance, the particles are too large and the wall confinement is too strong compared to what is typical of a real fluidized bed. Thus, our goal is to understand the fundamental physics, based on which one may hope to build more realistic models. In particular, the insights about how thermal effects modify suspension microstructure should be further investigated in multi-particle simulations and experiments.

Acknowledgment is made to the Donors of The Petroleum Research Fund, administered by the American Chemical Society, for partial support of this research. J. J. F. was also supported in part by a 3M Non-tenured Faculty Award and by an NSF Career Award. We thank Professors A. Acrivos, P. S. Ayyaswamy and G. Tryggvason for stimulating discussions, and Professors Shiyi Chen and Zhen-Su She and the State Key Laboratory for Turbulence Research at Peking University for sponsoring summer visits by J. J. F. and H. H. H., where part of the work was done.

REFERENCES

Acrivos, A. & Taylor, T. D. 1962 Heat and mass transfer from single spheres in Stokes flow. *Phys. Fluids* **5**, 387–394.

Aidun, C. K. & Lu, Y. 1995 Lattice Boltzmann simulation of solid particles suspended in fluid. *J. Statist. Phys.* **81**, 49–61.

Ayyaswamy, P. S. 1989 Combustion dynamics of moving droplets. *Encyclopedia of Environmental Control Technology* (ed. N. P. Cheremisinoff), vol. 1, pp. 479–532. Gulf Publishing Co.

Bellan, J. 1991 Liquid drop behavior in dense and dilute clusters. In *Numerical Approaches to Combustion Modeling* (ed. E. S. Oran & J. P. Boris), chap. 18. AIAA.

Bennon, W. D. & Incropera, F. P. 1987 A continuum model for momentum, heat and species transport in binary solid–liquid phase change heat systems. I. Model formulation. *Intl J. Heat Mass Transfer* **30**, 2161–2170.

Chang, M. W. & Finlayson, B. A. 1987 Heat transfer in flow past cylinders at $Re < 150$ – Part I. Calculations for constant fluid properties. *Numer. Heat Transfer* **12**, 179–195.

Chiang, C. H. & Sirignano, W. A. 1993 Interacting, convecting, vaporizing fuel droplets with variable properties. *Intl J. Heat Mass Transfer* **36**, 875–886.

Crowe, C. T. 1991 Overview of spray modeling. In *Numerical Approaches to Combustion Modeling* (ed. E. S. Oran & J. P. Boris), chap. 17. AIAA.

Dasgupta, S., Jackson, R. & Sundaresan, S. 1998 Gas-particle flow in vertical pipes with high mass loading of particles. *Powder Tech.* **96**, 6–23.

Delnoij, E., Kuipers, J. A. M. & van Swaaij, W. P. W. 1997 Computational fluid dynamics applied to gas–liquid contactors. *Chem. Engng Sci.* **52**, 3623–3638.

Dennis, S. C. R., Hudson, J. D. & Smith, N. 1968 Steady laminar forced convection from a circular cylinder at low Reynolds numbers. *Phys. Fluids* **11**, 933–940.

Feng, J., Hu, H. H. & Joseph, D. D. 1994 Direct simulation of initial value problems for the motion of solid bodies in a Newtonian fluid. Part 1. Sedimentation. *J. Fluid Mech.* **261**, 95–134.

Fortes, A. F., Joseph, D. D. & Lundgren, T. S. 1987 Nonlinear mechanics of fluidization of beds of spherical particles. *J. Fluid Mech.* **177**, 467–483.

Hao, Y. & Prosperetti, A. 2000 The collapse of vapor bubbles in a spatially non-uniform flow. *Intl J. Heat Mass Transfer* **43**, 3539–3550.

Hu, H. H., Joseph, D. D. & Crochet, M. J. 1992 Direct simulation of fluid particle motions. *Theoret. Comput. Fluid Dyn.* **3**, 285–306.

Hu, H. H. & Patankar, N. 1995 Non-axisymmetric instability of core-annular flow. *J. Fluid Mech.* **290**, 213–224.

Hu, H. H., Patankar, N. A. & Zhu, M. Y. 2001 Direct numerical simulations of fluid–solid systems using the arbitrary Lagrangian–Eulerian technique. *J. Comput. Phys.* **169**, 427–462.

Huang, L. J. & Ayyaswamy, P. S. 1987 Heat and mass transfer associated with a spray drop experiencing condensation: a fully transient analysis. *Intl J. Heat Mass Transfer* **30**, 881–891.

Ishii, M. 1975 *Thermo-fluid Dynamic Theory of Two-phase Flow*. Eyrolles.

Joseph, D. D. 1996 Flow induced microstructure in Newtonian and viscoelastic fluids. *Proc. 5th World Congr. Chem. Engng, San Diego*, vol. 6, pp. 3–16. AIChE.

Joseph, D. D., Liu, Y. J., Poletto, M. & Feng, J. 1994 Aggregation and dispersion of spheres falling in viscoelastic liquids. *J. Non-Newtonian Fluid Mech.* **54**, 45–86.

Juric, D. & Tryggvason, G. 1998 Computations of boiling flows. *Intl J. Multiphase Flow* **24**, 387–410.

Kovatcheva, N. T., Polyanin, A. D. & Kurdjumov, V. N. 1993 Mass transfer from a particle in a shear flow with surface reactions. *Acta Mechanica* **101**, 155–160.

Kuehn, T. H. & Goldstein, R. J. 1976 An experimental and theoretical study of natural convection in the annulus between horizontal concentric cylinders. *J. Fluid Mech.* **74**, 695–719.

Ladd, A. J. C. 1997 Sedimentation of homogeneous suspensions of non-Brownian spheres. *Phys. Fluids* **9**, 491–499.

Liu, Y. J., Nelson, J., Feng, J. & Joseph, D. D. 1993 Anomalous rolling of spheres down an inclined plane. *J. Non-Newtonian Fluid Mech.* **50**, 305–329.

Newman, B. G. 1961 The deflexion of plane jets by adjacent boundaries – Coanda effect. In *Boundary Layer and Flow Control* (ed. G. V. Lachmann), vol. 1, pp. 232–264. Pergamon.

Sadeghipour, M. S. & Razi, Y. P. 2001 Natural convection from a confined horizontal cylinder: the optimum distance between the confining walls. *Intl J. Heat Mass Transfer* **44**, 367–374.

Sadhal, S. S., Ayyaswamy, P. S. & Chung, J. N. 1997 *Transport Phenomena with Drops and Bubbles*. Springer.

Sasaguchi, K., Kusano, K. & Viskanta, R. 1997 A numerical analysis of solid–liquid phase change heat transfer around a single and two horizontal, vertically spaced cylinders in a rectangular cavity. *Intl J. Heat Mass Transfer* **40**, 1343–1354.

Schlichting, H. 1979 *Boundary-layer Theory*, 7th edn. McGraw-Hill.

Shin, S. & Juric, D. 2002 Modeling three-dimensional multiphase flow using a level contour reconstruction method for front tracking without connectivity. *J. Comput. Phys.* **180**, 427–470.

Sirignano, W. A. 1993 Formulation of spray combustion equations. In *Numerical Modelling in Combustion* (ed. T. J. Chung), chap. 9. Taylor & Francis.

Sirignano, W. A. 1999 *Fluid Dynamics and Transport of Droplets and Sprays*. Cambridge University Press.

Smith, D. N., Stiegel, G. J. & Ruether, J. A. 1987 Modeling three-phase reactor systems. *Encyclopedia of Fluid Mechanics* (ed. N. P. Cheremisinoff), vol. 6, pp. 535–682. Gulf Publishing Co.

Tirumkudulu, M., Tripathi, A. & Acrivos, A. 1999 Particle segregation in monodisperse sheared suspensions. *Phys. Fluids* **11**, 507–509.

Unverdi, S. O. & Tryggvason, G. 1992 A front-tracking method for viscous, incompressible, multi-fluid flows. *J. Comput. Phys.* **100**, 25–37.

White, F. M. 1991 *Viscous Fluid Flow*, 2nd edn. McGraw-Hill.